International Journal of Heat and Mass Transfer 124 (2018) 1015–1024

Contents lists available at ScienceDirect

International Journal of Heat and Mass Transfer

journal homepage: www.elsevier.com/locate/ijhmt

Experimental, numerical and analytic study of unconstrained melting in a vertical cylinder with a focus on mushy region effects

Chunjian Pan [a,*], Joshua Charles [a], Natasha Vermaak [a], Carlos Romero [a], Sudhakar Neti [a], Ying Zheng [b], Chien-Hua Chen [b], Richard Bonner III [b]

[a] Energy Research Center, Lehigh University, Bethlehem, PA 18015, USA
[b] Advanced Cooling Technologies, Inc., Lancaster, PA 17601, USA

ARTICLE INFO

Article history:
Received 15 February 2018
Received in revised form 30 March 2018
Accepted 2 April 2018

Keywords:
Enthalpy-porosity method
Mushy zone constant
Unconstrained melting

ABSTRACT

The enthalpy-porosity method is widely used in solving solid-liquid phase change problems that involve convection in the melt; however the influence of the required mushy zone parameter on the melting process has been largely overlooked. In this paper, further investigation of the mushy zone parameter is presented. The enthalpy-porosity method is the default model in Fluent for melting simulations. A comprehensive discussion of previously reported mushy zone parameter values is presented with a comparison to numerical and experimental results. In this paper, based on experimental validations of melting times, it is found that mushy zone parameters can be optimized based on relevant driving temperature differences. And despite the fact that the model cannot capture bulk solid sinking behaviors, numerical solid sinking behaviors by Fluent are still widely reported in the literature. Explanations and supporting numerical analysis are given for this seeming contradiction. Finally, an analytic solution for unconstrained sinking is developed. With the introduction of a tuning parameter to modify the viscosity of the mushy region in the bottom liquid layer, good agreement between the analytical model and experimental results is achieved. A linear correlation for the tuning parameter based on driving temperature differences is given.

1. Introduction

The enthalpy-porosity method [1], which is based on fixed grids, is the most popular modeling method for solid-liquid phase change problems that involve convection in the melt. It is the default method employed in the commercial computational fluid dynamics (CFD) code ANSYS Fluent. The enthalpy-porosity technique treats the mushy region (partially solidified region) as a porous medium. The porosity is set equal to the liquid fraction of the region. The fully solidified region has zero porosity and the phase change material (PCM) velocity approaches zero. To capture the mushy zone behavior, a source term is used to modify the momentum equation in the mushy region. The source term has the form [2]:

$$S = C\frac{(1-\alpha)^2}{(\alpha^3+\epsilon)}\vec{v}, \tag{1.1}$$

where ϵ is a small number (0.001) to prevent division by zero, α is the PCM liquid volume fraction, $\vec{v}$ is velocity field and C is the mushy zone parameter. In the liquid region ($\alpha = 1$), the source term has a zero value and the momentum equation describes the actual fluid velocities. In the mushy zone region, the moment equation approximates the Darcy law. A small C allows for significant flow and a large value suppresses the fluid velocities. In the solid region ($\alpha = 0$), the parameter C effectively forces the velocities to zero. However, when C is too small, i.e. $C = 10^2$, the solid PCM is treated like a highly viscous fluid. When C is too large, i.e. $C = 10^8$, the solid remains suspended in the liquid contrary to experimental findings that demonstrate the sinking of the solid PCM [3]. It is clear that the default enthalpy-porosity method within ANSYS Fluent [2] is incapable of modeling the bulk solid sinking behavior.

The influence and treatment of the mushy zone parameter on melting processes within the enthalpy-porosity method has been largely overlooked, despite the fact that the method is widely employed. Kumar and Krishna [4] numerically studied melting in a 2-D rectangular cavity by using the CFD code ANSYS Fluent 16.0. It was observed that the mushy zone constant had significant influence on the thermohydraulics of the melt PCM. As a result, the

* Corresponding author.
E-mail address: chp313@lehigh.edu (C. Pan).

https://doi.org/10.1016/j.ijheatmasstransfer.2018.04.009
0017-9310/

Nomenclature

S	a source term to modify the moment equation
C	mushy zone parameter
$\vec{v}$	velocity field, m/s
D	diameter of the cylinder, cm
w_s	thickness of the cylinder bottle wall, mm
w_b	thickness of the cylinder bottle bottom, mm
std	standard deviation, s
dT	driving temperature difference, °C
H	height, m
R	radius of solid PCM for the analytic solution, m
h	remaining height of solid PCM during analytic melting, m
r	shrinking radius of the solid PCM, m
T	temperature, °C
$u(r)$	flow velocity in the bottom liquid layer, m/s
$P(r)$	pressure distribution in the bottom liquid layer, Pa
z	height variable, m
M	tuning parameter for the viscosity in the mushy zone liquid layer
g	acceleration due to gravity, m/s^2
L_f	latent thermal energy of PCM, J/kg
L_e	virtual latent thermal energy of PCM, J/kg
Cp	heat capacity of PCM, J/kg K
k	conductivity of PCM, W/m K
X	liquid fraction of PCM
V	volume, m^3
t	time, min
x	width of a drawn vector box, cm
y	height of a drawn vector box, cm

Greek letters

$\in$	a small number to prevent division by zero
ρ	density of PCM, kg/m^3
μ	viscosity, Pa · s
δ	bottom liquid thickness, m
α	liquid volume fraction of PCM

Subscripts

l	liquid state
s	solid state
i	initial
m	melting
w	wall
c	cylinder
pcm	phase change material

melt fraction curve depends sensitively on the mushy zone parameter.

Assis et al. [5] studied melting in a spherical shell both experimentally and numerically. It was found that $C = 10^5$ showed solid sinking behavior in the simulations and fitted well to the experimental results. A commercial PCM, RT27, was used in his study and its viscosity is around 0.0035 Pa · s [6]. Hosseinizadeh et al. [7] also studied unconstrained melting in a spherical shell using n-octadecane, whose viscosity is 0.0039 Pa · s. It was also confirmed that $C = 10^5$ gave good agreement between the numerical and experimental results. Dari et al. [8] numerically studied unconstrained melting in a rectangular enclosure. With the mushy zone parameter C set at $C = 10^5$, solid sinking behaviors were observed. After Assis's work [5], many researchers [8–13,19] mentioned using a value of $C = 10^5$ for the mushy zone parameter when modeling PCM melting processes by the enthalpy-porosity method [1].

Mushy zone constants with some other values have also been reported in the literature. Tiari et al. [14] reported that with a mushy zone value $C = 2.5 \times 10^6$ the numerical results showed good agreement with previous experimental works. The PCM used in Tiari's work [14] is KNO_3, whose viscosity is 0.00259 Pa · s. Elbahjaoui and Qarnia [15] numerically studied melting of a paraffin wax (P116) dispersed with Al_2O_3 nanoparticles in a rectangular storage unit. The viscosity of P116 is 0.0013 Pa · s. A mushy zone value $C = 1.6 \times 10^6$ was used, which was reported to have good agreement with experimental results in the literature.

However, with these parameter values, disagreement between numerical and experimental results was also reported in the literature. Shmueli et al. [16] simulated PCM (RT27) melting in a vertical cylindrical tube, which was insulated at the bottom and exposed to air at the top and heated at the tube wall. The effect of the mushy zone parameter C on the simulation results was investigated. It was found that with $C = 10^5$, the resulting melting time by the simulation was about 2.5 times shorter than the experimentally measured time under the same conditions. A concern should be raised because the discrepancy could not be overcome by any changes of the mushy zone parameter and also material properties (such as the density and viscosity of the liquid phase) [16]. What's more disturbing is that in Assis's work looking at the spherical geometry [5], with the same PCM (RT27), good agreement between the numerical and experimental results was reported.

Thus a further look into the two cases is necessary. The most obvious differences between the cases are the geometry and the boundary conditions. For both of the cases, the PCM would sink towards the bottom of the container during the experiments, which will effectively reduce the thermal resistance between the solid PCM and the bottoms of the containers. However, for the vertical cylinder case [16], the bottom was insulated, so the solid sinking phenomenon would have small contribution to heat transfer enhancement. While for the sphere case [5], it was heated around the spherical shell, so the solid sinking phenomenon accelerated the melting process as demonstrated by the experimental melting patterns [5]. It can be argued that with the mushy zone parameter set to $C = 10^5$, the source term (Eq. (1.1)) generates suitable level of convection enhanced heat transfer in the liquid PCM, which agrees with the experiment. However, for the vertical cylinder case [16], one presumed conclusion is that the source term—with any value of the mushy zone parameter—always creates more convection in the liquid PCM than the real experimental situation when the solid sinking has a small role in enhancing the heat transfer.

Moreover, it is mentioned that the melting model in Fluent does not have the mechanism to model solid sinking. Ghasemi and Molki [17] numerically studied unconstrained melting in square cavities by a fixed-grid enthalpy formulation. In their work, to account for solid sinking, besides the natural convection source term in the momentum equation, the bulk solid sinking induced convection was expressed as a separate source term, which captures the sinking of the solid phase. It was found that when the sinking source term was set to zero, natural convection can also cause the solid to sink as the convection in the liquid phase can exert a downward shearing force on the solid. The two sources terms can achieve similar PCM melting patterns. However, studies [5,7,8] without such a source term also demonstrated that with a suitable mushy zone parameter value, solid sinking patterns were

observed by numerical analysis. Thus a suitable mushy zone parameter value is needed to match the numerical results by Fluent with the experimental ones [5,7]. This further concludes that the mushy zone parameter plays a vital role in modeling PCM melting by the enthalpy-porosity method [1]. It needs to be calibrated by experimental results for reliable numerical analysis.

From above discussions, further study on the mushy zone parameter is needed. In this paper, an experimental study of PCM melting in a vertical cylinder that is heated in a water bath is carried out. The PCM used in this paper is Calcium Chloride hexahydrate ($CaCl_2 \cdot 6H_2O$), whose viscosity is 0.01 $Pa \cdot s$, which is much larger than that of paraffin. Then numerical simulations with different values of the mushy zone parameter are compared to the experimental results. On the one hand, this study is used to confirm whether the numerical solution can match the experimental results when heat transfer is enhanced by the solid sinking behavior. On the other hand, it is desired to find a suitable mushy zone parameter value, which can be applied to PCM melting in a vertical cylindrical geometry with solid sinking phenomenon, as in the previous studies [5,7] that were based on a spherical geometry. Furthermore, whether the numerical model can capture the sinking phenomenon is discussed by comparing the numerical results with the experimental ones.

Finally, as the numerical method is incapable of modeling the sinking phenomenon, a modified analytic solution based on the bulk solid sinking phenomenon was developed. During earlier works, Moore and Bayazitoglu [20] studied contact melting of a PCM within a spherical enclosure. Their mathematical model was confirmed by experimental evidence. The contact melting process of solid materials on circular and rectangular heated plates was analyzed by Webb and Viskanta [21]. Chen et al. [22] developed an analytic solution for close-contact melting in a vertical tube with isothermal heating both at the side wall and the bottom. Close-contact melting of a PCM inside a heated rectangular capsule was also analytically studied by Chen et al. [23]. Yoo [24] analytically studied unsteady close-contact melting on a plate and showed that initially the melt height is far from constant. Kozak et al. [25] studied close-contact melting in vertical annular enclosures both numerically and analytically. Rozenfeld et al. [26] studied close-contact melting in a horizontal cylindrical enclosure with longitudinal plate fins. More recently, Zhao et al. [27] theoretically and experimentally studied close-contact melting in a rectangular cavity at different tilt angles. In this paper, considering the analytic model by Chen et al. [22] tends to under predict the melting time, a tuning parameter that can effectively controls the thickness of the bottom liquid layer is introduced in the development of the solution. With this tuning parameter, the analytical solution achieves good agreement with the experimental results.

The content of this paper is organized as follows. In Section 2, the experimental setup is introduced. In Section 3, numerical studies by Fluent are performed along with the determination of the mushy zone parameters to match the experimental results. Section 4 presents a new analytic solution. Section 5 summarizes the conclusions.

2. Experimental setup and results

In this paper, Calcium Chloride hexahydrate ($CaCl_2 \cdot 6H_2O$) was used for the experimental study of unconstrained melting. Fig. 1 shows the schematic of the experimental setup. It primarily consists of a controllable water bath, a GoPro camera, a light and a glass tube containing the PCM. During the experiment, the PCM tube is vertically suspended in the water bath. The GoPro is set to acquire a photo every 10 s, which allows the final melting time of one sample to be recorded. Before the experiment, the sample

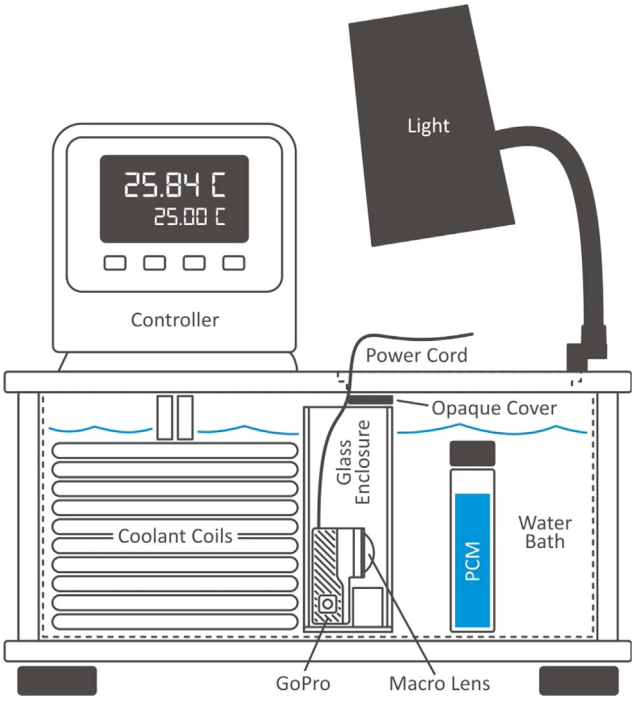

Fig. 1. Schematic diagram of the experimental setup.

Table 1
Samples.

Cases	H_{pcm} (cm)
#1 (10 g)	1.6237
#2 (20 g)	3.2474

was immersed in a separate water bath overnight with its temperature held at 24 °C. This temperature will be the initial temperature to be used in the numerical analyses.

Two samples (10 g & 20 g) were used to record the melting time. The height values in Table 1 are calculated based on the two weights and inner tube diameter. Multiple samples were prepared with the same weight. In addition, melting tests of these samples were repeated under three different driving temperature differences (10 °C, 15 °C and 20 °C). Table 4 shows the melting times, along with mean values and standard deviations (*std*) of the two sample weights under the three temperature differences. Fig. 2 shows the melting patterns of one case at different times. It can be seen that the solid shrinking happened much faster along the height than in the radial direction, which clearly demonstrate solid sinking can efficiently promote melting. Fig. 3 summarizes the experimental results.

3. Numerical study and discussions

Numerical studies were carried out using the commercial software ANSYS 16.0/Fluent. The 'volume-of-fluid' (VOF) model is used to describe the PCM-air system in the Fluent software. The VOF model treats two or more fluids as non-interpenetrating phases. To simulate the melting process, Fluent uses an enthalpy-porosity formulation by Voller et al. [2,18]. Extensive descriptions of the numerical models can be found in the literature [5,20]. Thus mathematical description is omitted in this paper.

Fig. 4 shows the computational domain to be simulated in Fluent, along with its dimensions in Tables 1 and 2. Constant temperature was applied to both the bottom and the side wall of the

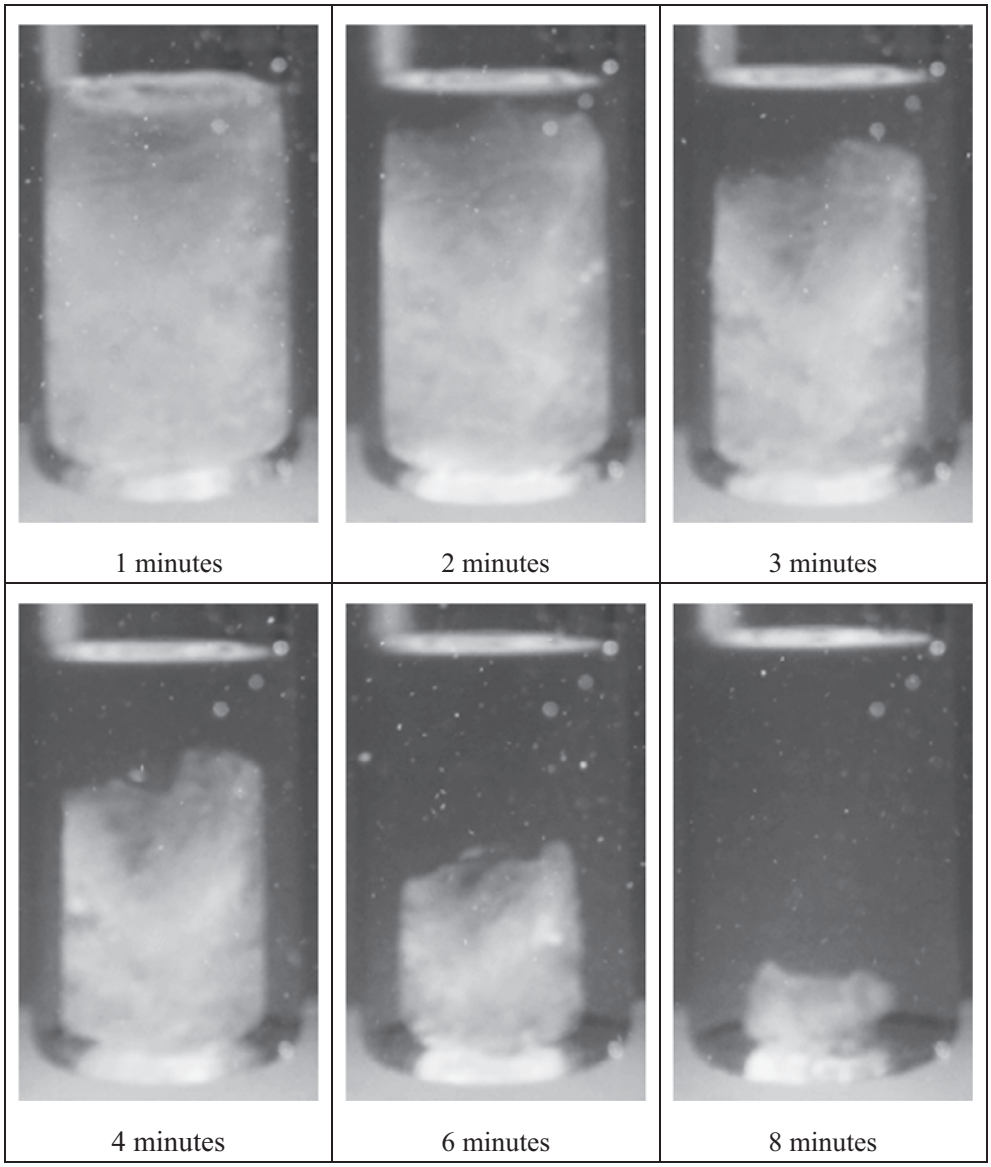

Fig. 2. Melting patterns under 20 °C temperature differences for Case # 2.

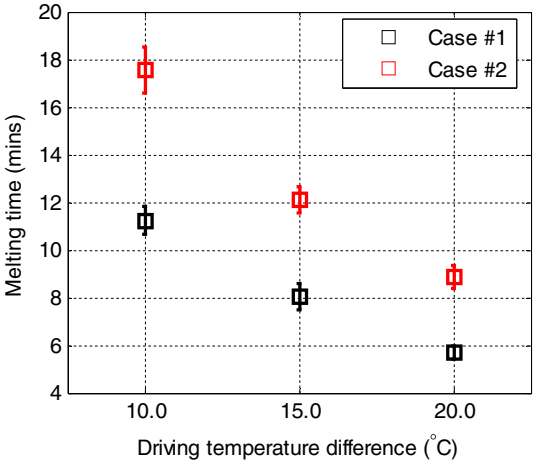

Fig. 3. Mean melting times & standard deviations of two sample weights under three temperature differences.

cylinder. The top of the cylinder is closed and is adiabatic. The properties of the glass tube are shown in Table 3. Properties of $CaCl_2 \cdot 6H_2O$ used in the simulations are shown in Table 5. The melting temperature range is (301–303 K). In the numerical simulations, as the difference of the specific heats of the solid and liquid phases is small, an average value 2145 J/kg K is used, which makes it easier to be implemented in the analytic solution. Piecewise linear functions were used for both the density and thermal conductivity (Table 6).

In the setting of the numerical model in Fluent, an explicit scheme was chosen for the volume fractions of air and PCM and a sharp interface between them was selected; the cutoff criterion is 1×10^{-7} and the Courant number is set to 0.25. The SIMPLE algorithm was used and second order upwind spatial discretization was chosen for both the momentum and energy equations. A quadrilateral grid structure was used for the mesh. According to the mesh and time step independence study shown in Fig. 5, an element size 0.2 mm and a time step of 0.01 s were chosen for all the following numerical simulations.

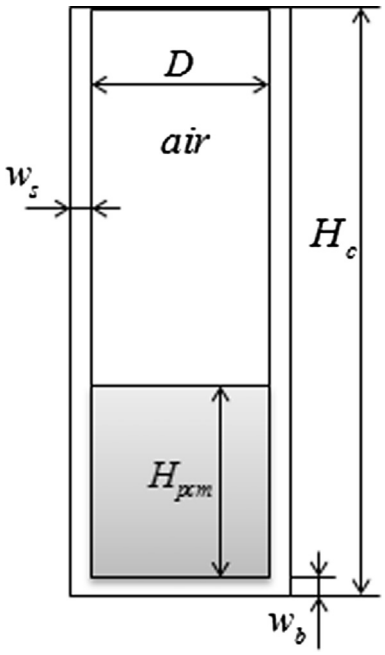

Fig. 4. Computational domain of the tube.

Table 2
Tube dimensions.

H_c	9.5 (cm)
D	2.258 (cm)
w_s	1.08 (mm)
w_b	1.0 (mm)

Table 3
Tube properties.

Density	2235 (kg/m^3)
Thermal conductivity	1.1 (W/m K)
Specific heat	800 (J/kg K)

Table 5
Thermophysical properties of $CaCl_2 \cdot 6H_2O$.

Properties	Values
Melting temperature	29 (°C)
Density (solid/liquid)	1706/1538 (kg/m^3)
Thermal Conductivity (solid/liquid)	1.09/0.546 (W/m K)
Specific heat (solid/liquid)	2060/2230 (J/kg K)
Latent heat	170 (kJ/kg)
Dynamic viscosity	0.01 Pa · s
Coefficient of thermal expansion	0.0005 K^{-1}

Table 6
Properties used in the simulations.

Temperature (K)	301	302	303
Density (kg/m^3)	1706	1622	1538
Conductivity (W/m K)	1.09	0.818	0.546

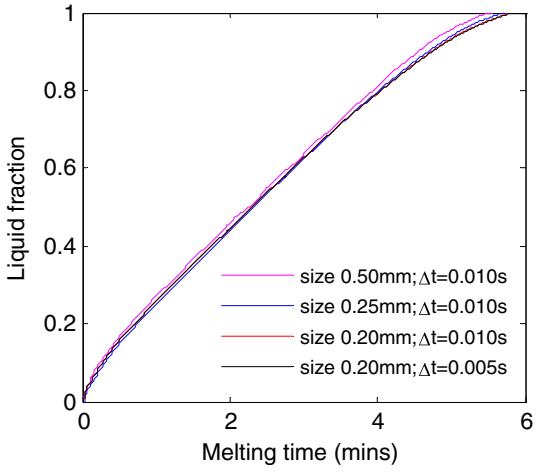

Fig. 5. Mesh and time step independence study.

To estimate the melt fraction throughout the melting process, images from the GoPro were imported into CorelDraw. CorelDraw is a vector-based design software package. Since the frames were taken at 10 s intervals, the time for each frame could be easily determined. After importing the images into CorelDraw, the images were scaled to the correct dimensions using the outside diameter of the bottle. Once scaled, a vector box was drawn over the solid portion of the PCM. The volume of this solid portion was calculated as $V_s = \left(\frac{x}{2}\right)^2 \pi y$, where x is the width of the drawn box and y is the height of the same box. At t = 0, V_s is assumed to be equal to 1. All V_s values for t > 0 are referenced to V_s (t = 0). Three repeated experimental data sets were used to estimate the liquid fraction during the melting for each case as shown in Figs. 6 and 7. The consistency of the liquid fractions for the same case by this method is acceptable.

Figs. 6 and 7 show liquid fraction curves of Case #1 with different values of the mushy zone constant under 10 °C and 20 °C driving temperature differences, respectively. It was found that for $dT = 10$ °C a mushy zone constant $C = 38 \times 10^5$ gives the best agreement with the experimental points. For $dT = 20$ °C, an

Table 4
Melting time for multiple samples under different temperature differences.

Cases	dT (°C)	Melting times (s)							
		1	2	3	4	5	6	mean	*std*
#1	10.0	680	700	710	680	610	660	673.33	35.59
#2		1140	1080	1080	1030	990	1000	1053.33	57.15
#1	15.0	440	450	480	500	510	520	483.33	32.65
#2		690	700	720	730	740	780	726.67	32.04
#1	20.0	360	360	330	320	330	350	341.67	17.22
#2		510	550	530	550	560	490	531.67	27.14

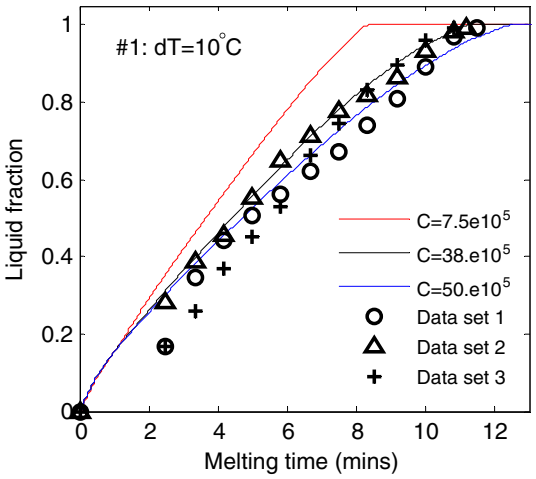

Fig. 6. Mushy zone constant study for Case 1 with 10 °C driving temperature difference.

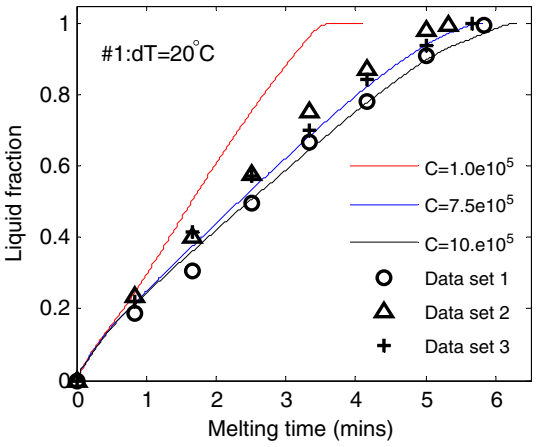

Fig. 7. Mushy zone constant study for Case 1 with 20 °C driving temperature difference.

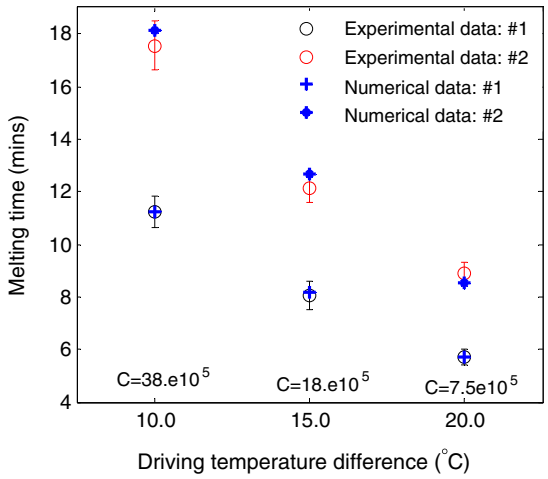

Fig. 8. Numerical and experimental melting times comparisons.

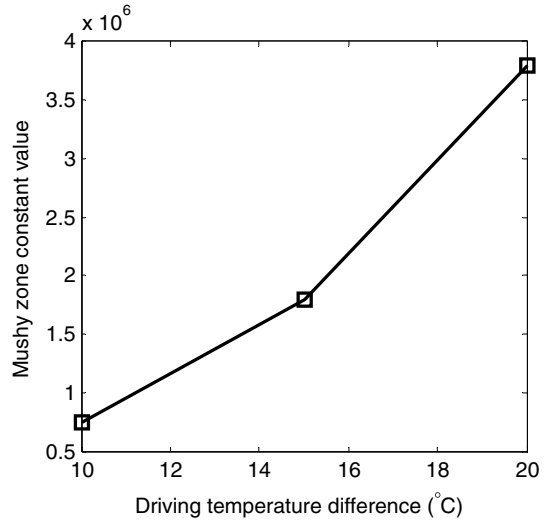

Fig. 9. Relationship between the driving temperature difference and verified mushy constant value.

optimal mushy zone constant is $C = 7.5 \times 10^5$. It seems that for different driving temperature differences, a different mushy zone constant is needed to match the numerical melting time with the experiment. This situation is further confirmed in Fig. 8. For $dT = 15$ °C, an optimal mushy zone constant is $C = 18 \times 10^5$. It can be seen that under the same driving temperature difference, with the same mushy zone constant, the numerical melting time for Case #2, which has a different mass of PCM and a different height-to-radius ratio than Case #1, shows good agreement with the experiments. Thus, it can be concluded that an optimal mushy zone constant is needed based on driving temperature difference when using Fluent to simulate melting. However, as indicated by Fig. 9, there is no strong linear relationship between the driving temperature difference and the mushy zone constant that is suggested by the experiments. A possible reason for this is that the differences in temperature gradients results in different magnitudes of natural convection, which affects the heat transfer performance in the liquid phase. Calibration with experiment is necessary to find a suitable mushy zone parameter value.

As a reminder, Shmueli [16] who also studied melting in a vertical cylindrical tube reported that no match can be found between the experimental and the numerical results for any value of the mushy zone parameter. The main difference is that with no bottom surface heating in Shmueli's [16] experiment, no heat transfer was promoted by the solid sinking phenomenon. Because of this, melting in the experiment happened much slower than the melting model in Fluent can predicted. When solid sinking promotes melting in the experiment, a match between the experiment and the numerical model was found with the optimal value of the mushy zone constant reported in [5,7].

Fig. 10 shows the numerical and experimental melting patterns. In terms of the solid fraction, the numerical and the experimental results show the same trend with time. No bulk solid sinking phenomenon is shown in the numerical fraction contours. However, the temperature contours seem to exhibit some sinking phenomenon. It is clear that the melting model in Fluent does not have the mechanism to capture the bulk solid downward movement. Nevertheless, in the mushy zone, due to the density difference, natural convection drives the heavier mushy components (partial solid) downward. Thus, relatively lower temperature at the bottom of the tube (blue[1] 'tailing' temperature contour) is observed through the melting process. This behavior to some degree mimics the contact melting phenomenon, as the incompletely melted solids fall

[1] For interpretation of color in Fig. 10, the reader is referred to the web version of this article.

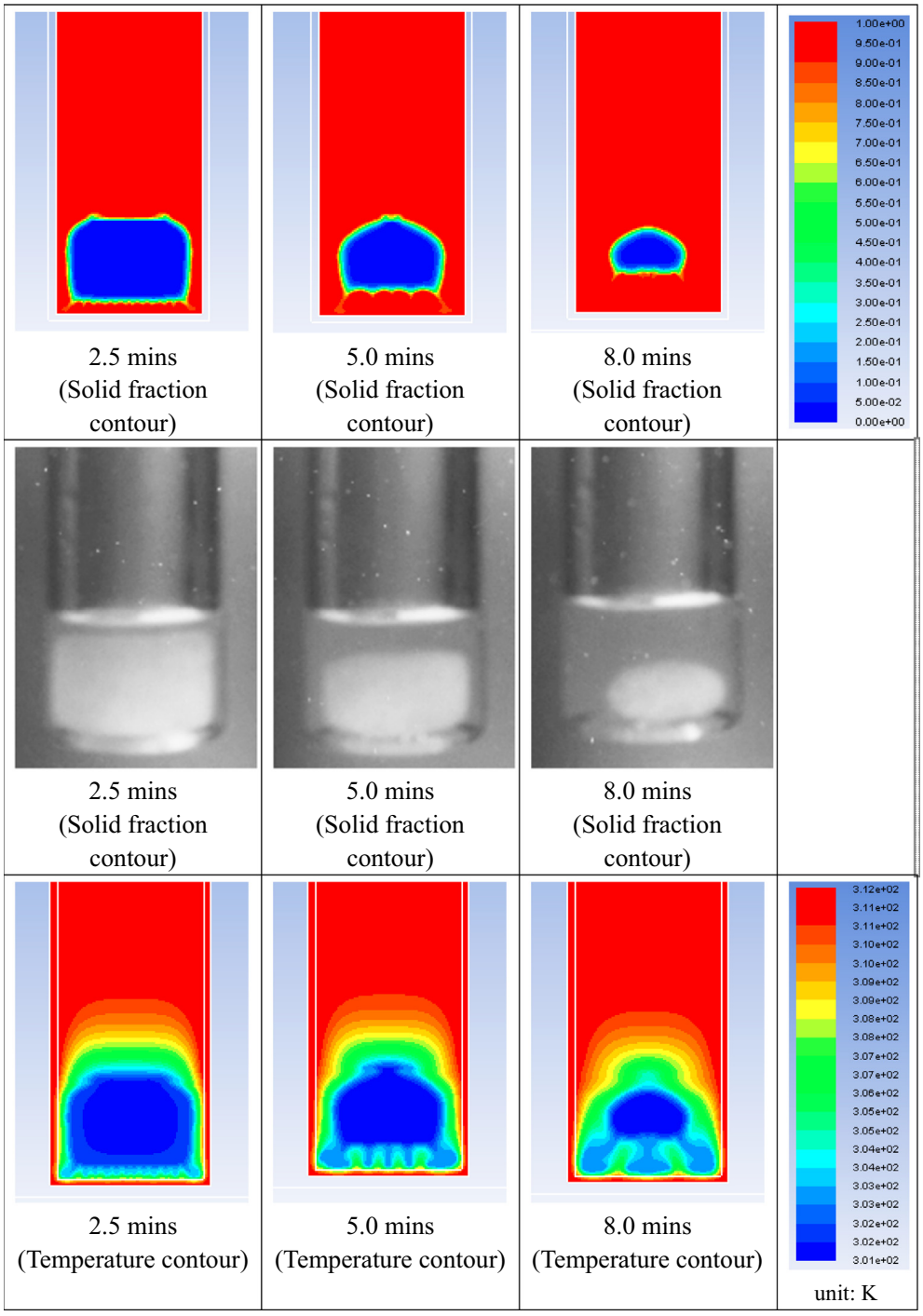

Fig. 10. Numerical and experimental melting patterns comparisons.

down to the bottom, although there is no differentiation between the solid and the liquid in the numerical approach. This may also explain the numerical sinking phenomenon reported in the literature [5,7,8] when using Fluent.

Furthermore, as the mushy zone parameter C controls the intensity of convection, especially in the mushy zone, C can affect the 'sinking' of the mushy components through natural convection, when the bottom surface is heated. This can be the reason that for each driving temperature difference, an optimal C is needed so that the numerical melting rate will be comparable to the experiment. However, when the bottom surface is insulated (no solid sinking to promote melting), the tuning of C is of no use due to the much slower melting process in the experiment [16]. When the bottom is heated, a good match can be achieved with a proper C value [5,7]. There are two probable reasons for the C values reported in this paper to be different from those in the literature [5,7]: one is the different viscosity, the other may be the differences in the bottom shape (flat versus curved). With a spherical bottom, heat transfer enhancement by solid sinking is more effective than the cylindrical shape in the current paper, resulting in a smaller mushy zone parameter ($C = 10^5$) for the numerical model to match the experiment.

4. A Modified analytic solution for unconstrained melting in a tube

The analytic solution proposed here for melting in a tube is based on contact melting analysis [20–24]. When PCM melts, a thin fluid layer with thickness δ is formed between the solid PCM and the bottom heating surface (Fig. 11). The heavier solid PCM tends to squeeze out the liquid and so δ remains thin. It is assumed that the process is quasi-steady, which means at every moment the weight of the solid is balanced by the pressure in the liquid film. Other assumptions include: (1) the temperature of the solid remains at the initial temperature; (2) heat transfer is dominated by conduction in the liquid film; (3) the liquid film has uniform thickness; (4) the flow in the liquid film is primarily parallel to the solid surface and driven by pressure gradients; (5) the inertia terms in the governing equations are neglected.

Based on these assumptions, Chen et al. [21] developed an analytic solution for close contact melting in a vertical tube with isothermal heating both at the side wall and the bottom. However, these assumptions are only valid when the solid phase is much denser than the liquid. It was found that the analytical model by Chen et al. [21] always tends to under predict the melting time. One most probable cause is the air voids in the solid PCM (observable during the experiments) that may significantly lower the melting rate. The analytic model does not include the thickness of the glass tube and the heat transfer coefficient between the water and the tube, which slightly underestimates the thermal resistance. The other possible cause is that the PCM ($CaCl_2 \cdot 6H_2O$) used in the experiment is of 98% purity. A sharp melting front may not be highly valid. Some transitional mushy zone could exist in the bottom liquid layer. Aiming at these situations that cannot be completely in accordance with the analytic model, a tuning parameter that can effectively adjust the thickness of the melt layer is introduced into the analytic solution. In this section, an analytic solution with a tuning parameter to adjust the thickness of the liquid layer is developed and its validation with experimental results is presented.

Fig. 11 shows the schematic of unconstrained melting in a cylinder. Assuming that the initial temperature is T_i everywhere, the PCM melting temperature is T_m and the cylinder is heated at the sides and the bottom with constant temperature T_w. The top boundary has zero heat flux.

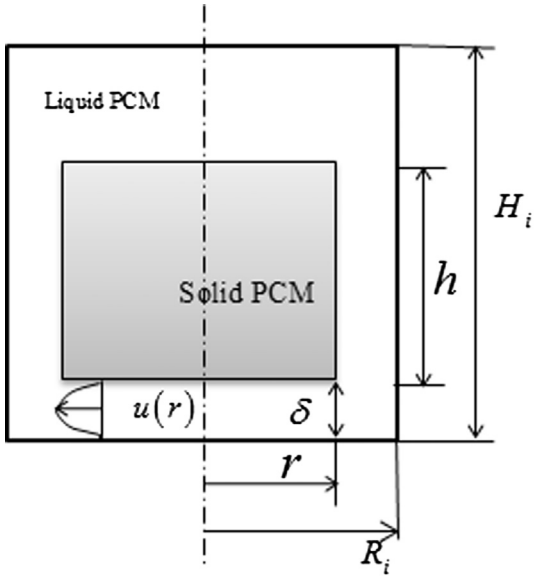

Fig. 11. Schematic of unconstrained melting.

First, a force balance acting on the solid PCM is considered. The momentum equation for the molten liquid layer at the bottom of the cylinder is:

$$\frac{dP}{dr} = \mu \frac{\partial^2 u(r)}{\partial z^2} \tag{3.1}$$

With boundary conditions: $u(r)|_{z=0} = 0$ & $u(r)|_{z=\delta} = 0$, its velocity is:

$$u(r) = \frac{1}{2\mu}\frac{dP}{dr}(z^2 - \delta z) \tag{3.2}$$

Mass balance equation at the bottom liquid layer can be written as:

$$\rho_l 2\pi r \int_0^{\delta} u(r)\mathrm{d}z = -\rho_s \frac{dh}{dt}\pi r^2 \tag{3.3}$$

Integrating Eq. (3.3) with respect to z, the pressure gradient is found to be:

$$\frac{dP}{dr} = \frac{6\mu}{\delta^3}\frac{\rho_s}{\rho_l}\frac{dh}{dt}r \tag{3.4}$$

The pressure gradient in the bottom melt layer plays an important role. Its force balance with the solid PCM will determine the thickness of the melt layer. When considering that there is a transitional region (mushy zone) during melting, the velocity given by Eq. (3.2) may no longer be valid. The existence of the mushy region will increase the flow resistance. Thus a tuning parameter can be introduced here to adjust the viscosity of the melt layer to mimic the extra flow resistance. The modified pressure gradient in the melt layer becomes:

$$\frac{dP}{dr} = \frac{6M\mu}{\delta^3}\frac{\rho_s}{\rho_l}\frac{dh}{dt}r \tag{3.5}$$

where M is the tuning parameter. Letting $\Phi = \frac{6M\mu}{\delta^3}\frac{\rho_s}{\rho_l}\frac{dh}{dt}$, and integrating Eq. (3.5) from 0 to r with respect to r:

$$\mathrm{P}(r) = \frac{\Phi}{2}r^2 + P(0) \tag{3.6}$$

The balance forces acting on the solid PCM can be described as:

$$\int_0^r 2\pi r P(r)dr = g(\rho_s - \rho_l)\pi r^2 h \tag{3.7}$$

Assuming $P(0) = 0$, Eq. (3.7) becomes:

$$\int_0^r r\Phi r^2 dr = g(\rho_s - \rho_l)r^2 h. \tag{3.8}$$

Solving Eq. (3.8) gives:

$$h = \frac{\Phi r^2}{4g(\rho_s - \rho_l)} \tag{3.9}$$

Second, in terms of energy balance, a linear temperature distribution within the liquid layer is assumed:

$$T = \frac{T_m - T_w}{\delta}\mathrm{z} + T_w, \tag{3.10}$$

which gives:

$$\left.\frac{dT}{dz}\right|_{z=\delta} = \frac{T_m - T_w}{\delta}, \tag{3.11}$$

To account for the sensible energy, an 'effective' latent heat capacity, L_e, is defined as:

$$L_e = L_f + Cp_s(T_m - T_i) + 0.5Cp_l(T_w - T_m) \tag{3.12}$$

The first term is the latent energy of the PCM, the second term is the sensible energy for the PCM temperature to increase from its initial value to the melting point and the third term accounts for the sensible energy in the liquid PCM, where the factor 0.5 is used to

approximate the temperature gradient within the liquid PCM. The local energy balance at the bottom solid PCM interface yields:

$$-k_l \left.\frac{dT}{dz}\right|_{z=\delta} = -\rho_s \frac{dh}{dt} L_e \tag{3.13}$$

With Eq. (3.11), the melt layer thickness can be obtained as:

$$\delta = \frac{k_l (T_w - T_m)}{-\rho_s \frac{dh}{dt} L_e} \tag{3.14}$$

Substituting Eq. (3.14) and the expression for Φ into Eq. (3.9), a differential equation for the time dependent solid PCM height h is obtained:

$$h = 6M\mu \frac{\rho_s}{\rho_l} \frac{(\rho_s L_f)^3}{4g(\rho_s - \rho_l)k_l^3 (T_w - T_m)^3} r^2 \left(\frac{dh}{dt}\right)^4 \tag{3.15}$$

Let $\Theta = 6M\mu \frac{\rho_s}{\rho_l} \frac{(\rho_s L_f)^3}{4g(\rho_s - \rho_l)k_l^3 (T_w - T_m)^3}$, and Eq. (3.15) is simplified as:

$$h = r^2 \Theta \left(\frac{dh}{dt}\right)^4 \tag{3.16}$$

Solving this differential equation by integration:

$$\int_{H_i}^{h} -(h)^{-1/4} dh = \int_0^t (r^2 \Theta)^{-1/4} dt \tag{3.17}$$

The final expression for the shrinking solid PCM height is:

$$h = \frac{3}{4}\left(\frac{4}{3}(H_i)^{3/4} - \int_0^t (r^2 \Theta)^{-1/4} dt\right)^{4/3} \tag{3.18}$$

For melting through the side wall of the vertical tube, it is assumed that no convection in the melt is considered. Hence, heat transfer is based on pure conduction. The energy balance equation can be written as followings:

$$\rho_s L_f (R_i - r)\frac{dr}{dt} = -\frac{k_l (T_m - T_w)}{ln((R_i - r)/R_i)} \tag{3.19}$$

Solving the equation by integration, an implicit form for the r (shrinking radius of the solid PCM) is obtained:

$$(R_i - r)^2 \left(2ln\left(\frac{R_i - r}{R_i}\right) - 1\right) = \frac{4k_l (T_w - T_m)t}{\rho_s L_f} \tag{3.20}$$

The analytic solution is obtained by solving Eqs. (3.20) and (3.18) in discrete time space. At each time step, r is calculated using Eq. (3.20) and is updated in Eq. (3.18) to calculate h. Finally, the liquid fraction is calculated as following:

$$X = \frac{\pi R_i^2 H_i - \pi r^2 h}{\pi R_i^2 H_i} \tag{3.21}$$

Fig. 12 shows the effects of the tuning parameter M on the bottom liquid thickness (δ). Fig. 12(a) shows that for the same case M can effectively control the thickness of δ. δ increases rapidly when all of the solid PCM is almost melted. Overall, a larger M tends to result in a thicker δ. Fig. 12(b) shows that for the same value M and the same dT, when the solid PCM has a higher height (#2), δ is smaller, which is consistent with physical intuition. The square dot points in Fig. 13 are the melting times estimated by the analytic solutions for the cases investigated in the experiments. It can be seen that for a given driving temperature, the experimental results for the two different geometries (#1 & #2) match the analytic solutions very well, with the same tuning parameter. The optimal tuning parameter has a strict linear relationship with the driving temperature differences ($M = 150$ for $dT = 10\,^{\circ}C$; $M = 100$ for $dT = 15\,^{\circ}C$; $M = 50$ for $dT = 20\,^{\circ}C$). Within this temperature range, a linear correlation for the tuning parameter based on driving temperature differences is given as:

$$M(dT) = 50 - 10(dT - 20), \quad 10\,^{\circ}C \leqslant dT \leqslant 20\,^{\circ}C \tag{3.22}$$

Finally, Fig. 14 presents a comparison of the melting curves between the experimental, the analytic and the numerical results. The experimental time- dependent liquid fraction curves for the two driving temperature differences were obtained based on the mean values of the three sets of data of each case as shown in Figs. 6 and 7. The numerical curves have a good agreement with

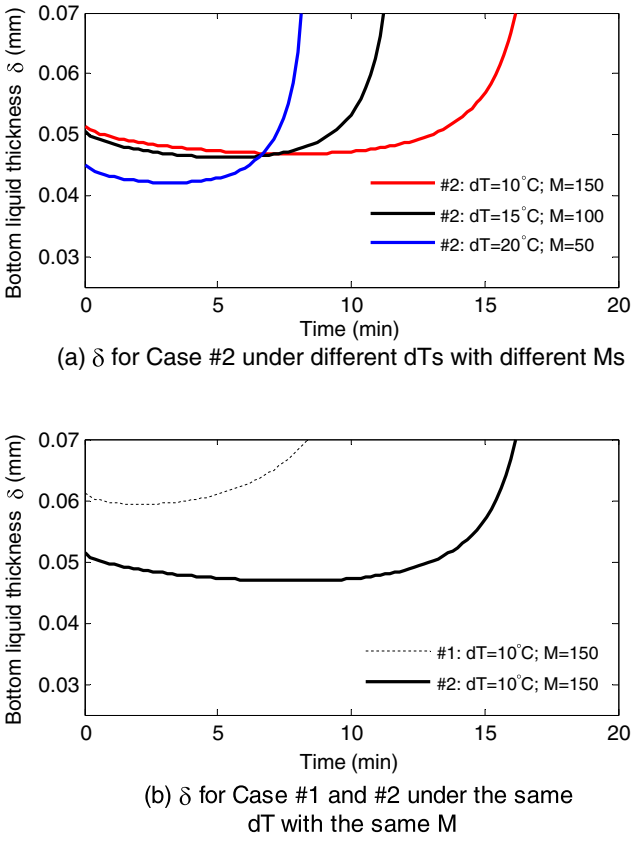

Fig. 12. Effect of the tuning parameter on the bottom liquid thickness.

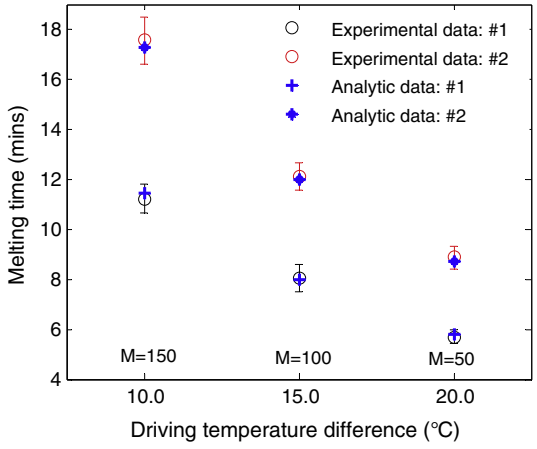

Fig. 13. Comparison of the melting times predicted by the analytic solution with the experimental results.

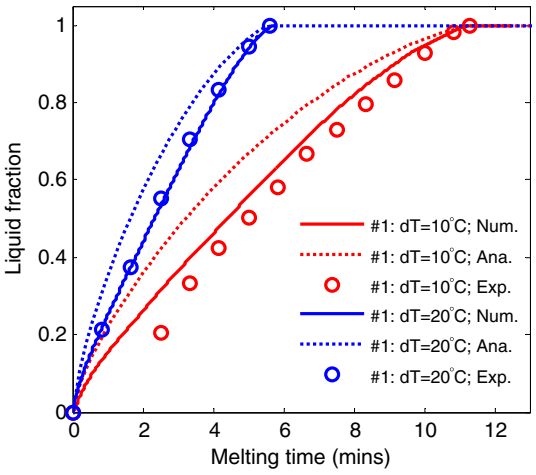

Fig. 14. Comparison of melting curves from the analytic and numerical solutions.

the experimental ones. Especially for the larger dT case, there is a perfect match. Although the analytic curves match with the experimental ones in terms of the final melting time, there is deviation during the middle of the melting process. The analytic solution gives faster melting at the beginning, while the experimental melting curve shows more linearity. Thus improvement of the analytic solution is still required for future studies.

5. Conclusions

The mushy zone parameter within the source term used to modify the moment equation for the enthalpy-porosity method is given more insight and discussion. In particular, the seeming contradiction that although, the enthalpy-porosity method in Fluent cannot model bulk solid sinking behavior, numerical solid sink behaviors are still reported in the literature. One possible explanation is that convection in the liquid phase can exert a downward shearing force on the solid. The other explanation is that within the mushy region, incompletely melted solids sink to the bottom by natural convection, which mimics the contact melting and enhances heat transfer. Moreover, in this paper, experiments demonstrating the melting of $CaCl_2 \cdot 6H_2O$ in a vertical tube submerged in a water bath are conducted and used to calibrate numerical models. It is proposed for the first time in this paper that it is necessary to optimize the mushy zone parameter based on relevant driving temperature differences in order to achieve good agreement between numerical melting times and experimental ones. Finally, an analytic solution for unconstrained melting in a vertical tube with a tuning parameter to modify the viscosity of the mushy region was developed. A linear correlation for the tuning parameter based on driving temperature differences is given and experimentally validated.

Conflict of interest

The authors declared that there is no conflict of interest.

Acknowledgement

This research is sponsored by the ARPA-e ARID Program under Contract No. DE-AR0000582. Any opinions, findings, and conclusions or recommendations expressed in this article are those of the authors and do not necessarily reflect the views of the Advanced Research Projects Agency-Energy.

References

[1] V.R. Voller, C. Prakash, A fixed grid numerical modeling methodology for convection-diffusion mushy region phase-change problems, Int. J. Heat Mass Transf. 30 (1987) 1709–1719.
[2] V.R. Voller, M. Cross, N.C. Markatos, An enthalpy method for convection/diffusion phase change, Int. J. Numer. Methods Eng. 24 (1987) 271–284.
[3] Y. Kozak, G. Ziskind, Novel enthalpy method for modeling of PCM melting accompanied by sinking of the solid phase, Int. J. Heat Mass Transf. 112 (2017) 568–586.
[4] M. Kumar, D. Jaya Krishna, Influence of mushy zone constant on thermohydraulics of a PCM, Energy Proc. 109 (2017) 314–321.
[5] E. Assis, L. Katsman, G. Ziskind, R. Letan, Numerical and experimental study of melting in a spherical shell, Int. J. Heat Mass Transf. 50 (9–10) (2007) 1790–1804.
[6] G. Ferrer, S. Gschwander, A. Solé, C. Barreneche, A. Inés Fernández, Peter Schossig, Lusia F. Cabeza, Empirical equation to estimate viscosity of paraffin, J. Storage Mater. 11 (2017) 154–161.
[7] S.F. Hosseinizadeh, A.A. Rabienataj Darzi, F.L. Tan, J.M. Khodadadi, Unconstrained melting inside a sphere, Int. J. Therm. Sci. 63 (2013) 55–64.
[8] A.R. Darzi, H.H. Afrouzi, M. Khaki, M. Abbasi, Unconstrained melting and solidification inside rectangular enclosure, J. Fundam. Appl. Sci. 7 (3) (2015) 436–451.
[9] R. Pakrouh, M.J. Hosseini, A.A. Ranjbar, R. Bahrampoury, A numerical method for PCM-based pin fin heat sinks optimization, Energy Convers. Manage. 103 (2015) 542–552.
[10] A.A. Al-Abidi, S. Mat, K. Sopian, M.Y. Sulaiman, A.Th. Mohammad, Internal and external fin heat transfer enhancement technique for latent heat thermal energy storage in triplex tube heat exchangers, Appl. Therm. Eng. 53 (1) (2013) 147–156.
[11] H. Eslamnezhad, A.B. Rahimi, Enhance heat transfer for phase-change materials in triplex tube heat exchanger with selected arrangements of fins, Appl. Therm. Eng. 113 (2017) 813–821.
[12] N. Das, Y. Takata, M. Kohno, S. Harish, Melting of graphene based phase change nanocomposites in vertical latent heat thermal energy storage unit, Appl. Therm. Eng. 107 (2016) 101–113.
[13] N. Das, Y. Takata, M. Kohno, S. Harish, Effect of carbon nano inclusion dimensionality on the melting of phase change nanocomposites in vertical shell-tube thermal energy storage unit, Int. J. Heat Mass Transf. 113 (2017) 423–431.
[14] S. Tiari, S. Qiu, M. Mahdavi, Numerical study of finned heat pipe-assisted thermal energy storage system with high temperature phase change material, Energy Convers. Manage. 89 (2015) 833–842.
[15] R. Elbahjaoui, H. El Qarnia, Transient behavior analysis of the melting of nanoparticle-enhanced phase change material inside a rectangular latent heat storage unit, Appl. Therm. Eng. 112 (2017) 720–738.
[16] H. Shmueli, G. Ziskind, R. Letan, Melting in a vertical cylindrical tube: numerical investigation and comparison with experiments, Int. J. Heat Mass Transf. 53 (19–20) (2010) 4082–4091.
[17] B. Ghasemi, M. Molki, Melting of unfixed solids in square cavities, Int. J. Heat Fluid Flow 20 (4) (1999) 446–452.
[18] A.D. Brent, V.R. Voller, K.J. Reid, Enthalpy-porosity technique for modeling convection-diffusion phase change: application to the melting of a pure metal, Num. Heat Transfer 13 (1988) 297–318.
[19] V. Shatikian, G. Ziskind, R. Letan, Numerical investigation of a PCM-based heat sink with internal fins, Int. J. Heat Mass Transf. 48 (2005) 3689–3706.
[20] F. Moore, Y. Bayazitoglu, Melting within a spherical enclosure, J. Heat Trans. 104 (1) (1982) 19–23.
[21] B.W. Webb, R. Viskanta, Natural-convection-dominated melting heat transfer in an tiltd rectangular enclosure, Int. J. Heat Mass Trans. 34 (12) (1991) 3097–3106.
[22] W. Chen, S. Cheng, et al., Study of contact melting inside isothermally heated vertical cylindrical capsules, J. Therm. Sci. 2 (3) (1993) 190–195.
[23] W. Chen, S. Cheng, Z. Luo, et al., Analysis of close-contacting melting of phase change materials inside a heated rectangular capsule, Int. J. Energy Res. 19 (4) (1995) 337–345.
[24] H. Yoo, Analytical solutions to the unsteady close-contact melting on a flat plate, Int. J. Heat Mass Transf. 43 (8) (2000) 1457–1467.
[25] Y. Kozak, T. Rozenfeld, G. Ziskind, Close-contact melting in vertical annular enclosures with a non-isothermal base: theoretical modeling and application to thermal storage, Int. J. Heat Mass Transf. 72 (2014) 114–127.
[26] T. Rozenfeld, Y. Kozak, R. Hayat, G. Ziskind, Close-contact melting in a horizontal cylindrical enclosure with longitudinal plate fins: demonstration, modeling and application to thermal storage, Int. J. Heat Mass Transf. 86 (2015) 465–477.
[27] J. Zhao, J. Zhai, Y. Lu, N. Liu, Theory and experiment of contact melting of phase change materials in a rectangular cavity at different tilt angles Int, J. Heat Mass Transfer. 120 (2018) 241–249.